DOI: 10.1002/ejic.201100599

Alkali Metal/Lanthanoid Heterobimetallic Complexes of 8-Hydroxyquinolines Accessed by Pseudo-Solid-State Reactions

Glen B. Deacon,*[a] Tobias Dierkes,[a][‡] Marcel Hübner,[a][‡] Peter C. Junk,*[a] Yvonne Lorenz,[a][‡‡] and Aron Urbatsch[a]

Keywords: Lanthanides / Alkali metals / Quinolinolates / Heterometallic complexes / Metal–organic frameworks

The heterobimetallic 1D-polymeric alkali metal/lanthanoid $[AMLn(Q)_4]_n$ [Q = OQ (8-quinolinolate): AM = Li, Ln = Tb, Ho, Er; AM = K, Ln = Er; Q = MQ (2-methyl-8-quinolinolate): AM = Rb; Ln = Tb, Er] complexes were obtained after rearrangement reactions between AM(Q) and $Ln(Q)_3$ in a 1,2,4,5-tetramethylbenzene flux at elevated temperatures. In these compounds, the eight-coordinate lanthanoid ion is surrounded by four (O, N) chelating Q ligands, which bridge to the adjacent alkali metal through their oxygen atoms to form the linear polymers. Dimeric $[Cs_2(MQ)_2(HMQ)_2]$ was obtained from an attempt to prepare $[CsEr(MQ)_4]_n$, and the caesium atoms are each ligated by one terminal HMQ and one chelating-bridging MQ ligand. In addition, the chelating-bridging ligands in $[Cs_2(MQ)_2(HMQ)_2]$ and in the rubidium derivatives $[RbLn(MQ)_4]_n$ (Ln = Tb, Er) exhibit bonding of the π-electron system to coordination saturate the large ionic alkali metal ion. The reaction of $Yb(MQ)_3$ in the presence of $K_2C_2O_4{\cdot}H_2O$ afforded the monomeric heterobimetallic $[KYb_2(MQ)_7]$ complex in which the three metal atoms are arranged in a triangular fashion. They are surrounded by seven MQ ligands, which display the previously encountered chelating (O, N) and the chelating-bridging μ-κ^2(N,O):κ^1(O) and μ_3-κ^2(N,O):κ^1(O):κ^1(O) ligation modes. Heating K(OQ) in 1,2,3,4-tetrachlorobenzene gave crystals of 8-hydroxyquinolinium chloride. The structure of $[Na_4(OQ)_4(H_2O)_8]_n$, obtained by neutralisation, has sodium ions coordinated by one chelating OQ and four aqua ligands, the latter bridge to adjacent sodium ions to give a double stranded 2D-polymer.

Introduction

The insolubility of lanthanoid derivatives of 8-quinolinol (HOQ) and 2-methyl-8-quinolinol/8-quinaldinol (HMQ) is an advantage for their use in gravimetric and volumetric analysis of the Ln elements,[1,2] but is a major disadvantage for obtaining crystals for structure determination. Besides being of intrinsic interest, the structures provide a basis for understanding physical properties. Erbium 8-quinolinolate shows luminescence in the near infrared region,[3–5] making it of interest for telecommunication and optical amplifier applications [also see the prominent electroluminescent $Al(OQ)_3$[6]]. The luminescence was initially interpreted on the basis of a monomeric six-coordinate structure,[3,4] whereas it was subsequently shown that the compound has a trinuclear arrangement, as shown by crystallisation as $[Er_3(OQ)_9]{\cdot}$MeCN.[5] This and the analogous $[Ho_3(OQ)_9]{\cdot}$HOQ[7] are the sole crystallographically characterised homoleptic lanthanoid 8-quinolinolate or 8-quinaldinolate complexes, illustrating the difficulty in accessing single crystals. Enhancement of solubility has been achieved by halogen[8a] or nitro[8b] substitution in OQ, by introduction of co-ligands,[8a,9] by formation of anionic complexes (and halogen substitution)[8a,8b] and by coordination of unionised MQ, leading to determination of the structures of $[Ln_3Q_8(OAc)]$ (Ln = Yb, Q = OQ;[9] Ln = Er, Q = 5-chloro-8-quinolinolate[8a]) as chloroform solvates, $[La_3(MQ)_8(NO_3)HMQ]{\cdot}4MeOH$,[10] $[ErQ_3(H_2O)_2]_2$ (Q = 5,7-dibromo- and 5,7-dichloro-8-quinolinolate),[5b] $\{[NH_4][ErQ_4]\}$ (Q = 5,7-dibromo-8-quinolinolate)[8a] and $[Sc(MQ)_3(HMQ)]{\cdot}(H_2O)$.[11] More elaborate functionalisation has both enhanced solubility and synthesis and also gives rise to luminescent and light-emitting materials, including heterobimetallic compounds,[12] for example, alkali metal/lanthanoid complexes of highly functionalised (partly to achieve solubility) OQ ligands have recently been reported and show bright near-infrared luminescence.[13] The rare earth/alkaline earth[14–16] and rare earth/transition metal heterobimetallic complexes $[Ln_2AE(MQ\text{ or }OQ)_8]$ and $[LnTM_2(OQ)_7]$[15,17] are also highly insoluble, posing similar synthesis and crystallisation problems to homometallic lanthanoid OQ and MQ complexes. We have, however, developed pseudo-solid-state syntheses, for example, reactions of the mixed metals[14] or alloys,[17] with HOQ and rearrangement reactions of $Ln(OQ\text{ or }MQ)_3$ and $AE(OQ\text{ or }MQ)_2$[15,16] or $TM(OQ)_2$[15] species at elevated temperatures (150–300 °C), alone or in a 1,2,4,5-tetrameth-

[a] School of Chemistry, Monash University, Clayton, VIC 3800, Australia
[‡] On exchange from: Fachbereich Chemieingenieurwesen, Fachhochschule Münster, Stegerwaldstrasse 39, 48565 Steinfurt, Germany
[‡‡] On exchange from: Fachgruppe Chemie, Rheinische Friedrich-Wilhelms-Universität, Gerhard-Domagk-Str.1, 53121 Bonn, Germany

 WILEY ONLINE LIBRARY © 2011 Wiley-VCH Verlag GmbH & Co. KGaA, Weinheim

ylbenzene (TMB) flux, to obtain single crystals of these compounds, particularly $[Ln_2AE(MQ)_8]$ and $[Eu_3Ba(MQ)_{11}]$ complexes.[16] Although the yields of single crystals are generally low (a not unfamiliar problem in solid-state chemistry), the bulk powder also can contain the heterobimetallic complexes, as revealed by powder X-ray diffraction. We have now developed these syntheses to yield heterobimetallic lanthanoid/alkali metal coordination polymers of the type $[AMLn(Q)_4]_n$ (Q = OQ or MQ) and the monomeric $[KYb_2(MQ)_7]$ and report their preparations and structures. A feature of the structures of $[RbLn(MQ)_4]_n$ complexes is π-interactions between the MQ ligands and Rb. Structures of a NaOQ and a CsMQ complex are also reported. Relatively few structures of alkali metal OQ or MQ complexes are known, but see $[Li_6(OQ)_6]$,[18a] $[Li_6(MQ)_6]$[18b] and [K(OQ)(HOQ)][19] for some examples.

Results and Discussion

Rearrangement reactions between alkali (AM) and lanthanoid (Ln) quinolinolates, "AM(Q)" and "$Ln(Q)_3$", [Q = 8-quinolinolate (OQ) or 2-methyl-8-quinolinolate (MQ)], the latter obtained from the reaction of stoichiometric amounts of lanthanoid salt and sodium quinolinolate, in a TMB flux at elevated temperatures (150–270 °C) led to the isolation of a series of 1D-polymeric heterobimetallic $[AMLn(Q)_4]_n$ [(Q = OQ: AM = Li, Ln = Tb (**1**), Ho (**2**), Er (**3**); AM = K, Ln = Er (**4**); Q = MQ: AM = Rb, Ln = Tb (**5**), Er (**6**)] complexes (Scheme 1). Crystalline material was handpicked from the bulk residual powder after the reaction. The low yield of crystalline material (a typical problem with solid-state syntheses) was prohibitive of characterisations other than single-crystal X-ray crystallography and IR spectroscopy in most cases, but powder diffraction X-ray crystallography was conducted for the $[AMLn(OQ)_4]_n$ series of complexes and demonstrated that the heterobimetallic complexes were present in the bulk powders. Decomposition of the bulk material in the MQ cases prohibited any similar approach. Obtaining samples suitable for elemental analysis was difficult because of the adherence of powder to the single crystals, which could not be recrystallised owing to insolubility arising from their polymeric structures. In some cases visually suitable samples were separated from suspensions in X-ray mounting oil (see the Experimental Section), although the analytical results were rather variable. Functionalisation of OQ provides access to soluble AM/Ln/Q derivatives, see for example ref.[13] but the challenges posed by parent OQ and MQ complexes and the novel structures obtained warrant their exploration.

$$\text{'AM(Q)' + 'Ln(Q)}_3\text{'} \xrightarrow{\text{TMB}} [AMLn(Q)_4]_n$$

Scheme 1. Reaction between "AM(Q)" and "$Ln(Q)_3$" in 1,2,4,5-tetramethylbenzene (TMB) in an evacuated tube at elevated temperature.

An attempted reaction between $Er(MQ)_3$ and Cs(MQ) afforded the crystalline homometallic dimer $[Cs_2(MQ)_2(HMQ)_2]$ (**7**). Another attempted reaction between $Eu(OQ)_3$ and Li(OQ) produced single crystals of the known hexameric $[Li_6(OQ)_6]$[18a] in low yield.

As was demonstrated by the isolation of $[Eu_3(MQ)_7CO_3]$[16] from a reaction involving $Eu(MQ)_3$ and $CaCO_3$, the elevated-temperature, pseudo-solid-state syntheses have potential to give heteroleptic lanthanoid 8-quinaldinolates. The reaction between $Yb(MQ)_3$ and $K_2C_2O_4{\cdot}H_2O$, in a 1:2 ratio, however, did not give a mixed MQ/C_2O_4 complex, but instead yielded the tri-nuclear homoleptic heterobimetallic complex $[KYb_2(MQ)_7]$ (**8**). This monomeric complex is structurally very different from the polymeric alkali/lanthanoid $[AMLn(Q)_4]_n$ complexes (below). A plausible formation reaction is proposed in Scheme 2. Powder XRD measurements on the bulk material suggested the presence of complex (**8**), but lines of residual potassium oxalate were dominant.

$$14\ Yb(MQ)_3 + 3\ K_2C_2O_4 \xrightarrow{\text{TMB}} 6\ [KYb_2(MQ)_7] + Yb_2(C_2O_4)_3$$

Scheme 2.

The incorporation of potassium rather than oxalate led to examination of the $Yb(MQ)_3/CaCO_3$ reaction. Only single crystals of HMQ were obtained but the bulk powder showed an X-ray diffractogram with features similar to those of $[Er_3(MQ)_7CO_3]$ {prepared from $Er(MQ)_3$ and $Ca(MQ)_2$[16]}, hence $[Yb_3(MQ)_7CO_3]$ was possibly formed.

Yellow single crystals of the new $[Na_4(OQ)_4(H_2O)_8]_n$ (**9**) were isolated upon concentrating a combined solution of HOQ and NaOH in ethanol. Previously, only the above-mentioned hexakislithium OQ complex $[Li_6(OQ)_6]$[18] and [K(OQ)(HOQ)][19] were known for unsubstituted OQ. (For alkali metal complexes of functionalised derivatives of OQ, see for example refs.[18b,20–23]) In an attempt to obtain crystals of K(OQ) by heating the compound in a 1,2,3,4-tetrachlorobenzene flux, only crystalline 8-hydroxyquinolinium chloride (**10**) was obtained and in very low yield.

Structural Discussion

The complexes $[AMLn(OQ)_4]_n$ [AM = Li; Ln = Tb (**1**), Ho (**2**), Er (**3**)] crystallise in the tetragonal space group *P*4/*ncc*, whilst $[KEr(OQ)_4]_n$ (**4**) crystallises in the monoclinic space group *P*2/*n*. In **1**–**4**, the lanthanoid atom is surrounded by four chelating (N, O) OQ ligands forming eight coordinate $[Ln(OQ)_4]^-$ moieties, with pairs of the 8-quinolinolate ligands bridging through their oxygen atoms to adjacent alkali metals to form the $[AMLn(OQ)_4]$ units. These heterobimetallic units connect to adjacent units to form the polymeric 1D chains, which propagate along the *c*-axis (**1** and **3**) and the *b*-axis (**4**) of the unit cell (Figure 1). The formation and structure of **2** was indicated by unit cell comparison and microanalysis. The analogous MQ derivatives $[RbLn(MQ)_4]_n$ [Ln = Tb (**5**), Er (**6**)] are different from these in that they crystallise in the orthorhombic space group *Pccn*. Furthermore, each $[RbLn(MQ)_4]$ unit is rotated around the Rb–Ln axis by 90° with respect to the adjacent

 © 2011 Wiley-VCH Verlag GmbH & Co. KGaA, Weinheim

unit within the polymeric strands (Figure 2). The other major difference from the OQ derivatives is that the larger alkali metal rubidium has a higher coordination number (CN) than the corresponding four-coordinate alkali metal in the OQ derivatives in which they have a distorted tetrahedral stereochemistry. The higher coordination number is achieved by involvement of the π-system of the ligands [C(8 and 9)–Rb < 3.5 Å] and bridging by nitrogen atoms (see below; Figure 2). This cut-off is supported by ranges for π-bonding of arenes to potassium[24] adjusted by the differences between the ionic radii of K^+ and Rb^+.[25,26] The average distance between carbon atoms of π-bonded arenes and potassium is 3.14 Å, and for rubidium this distance is 3.35 Å.[25] Complexes **5** and **6** have structures reminiscent of the $[AMLn(tBu_2pz)_4]_n$ class of complex (AM = Na, Ln = La, Tb, Ho, Er, Yb; AM = K, Ln = La, Nd, Sm, Tb, Ho, Er, Yb, Lu; tBu_2pz = 3,5-di-*tert*-butylpyrazolate), which were synthesised by metathesis, solventless or in an inert flux, at elevated temperatures (200–300 °C).[24]

The high symmetry of complexes **1**–**4** leads to the small number of unique bond lengths (Table 1). In the lithium derivatives, Ln–O bond lengths are 0.018 Å shorter in **3** than in **1**; in the potassium derivative **4**, the bond lengths are 0.037 Å shorter than in **1**, with the difference being close to that expected from the lanthanoid contraction when changing from terbium to erbium.[26] The larger size of the potassium ion in $[KEr(OQ)_4]_n$ (**4**) leads to shorter Ln–O (by 0.025 Å) and elongated Ln–N (by 0.036 Å) bond lengths, when compared with $[LiEr(OQ)_4]_n$ (**3**). The Ln–N bond lengths in **4** (Table 1) are equal to that in **1** [2.558(3) Å]. The larger size of the potassium ion compared with lithium leads to the $[Ln(OQ)_4]$ units being eclipsed when viewed along the metal–metal axis of the polymeric strand [Figure 1(b) right]; they do not interdigitate with adjacent units. The metal–metal distance in $[KEr(OQ)_4]_n$ (**4**) is 0.50 Å longer than in **1** and **3**, which in the last two cases remains little affected by the change of the lanthanoid metal (0.016 Å difference). As a consequence of the shorter

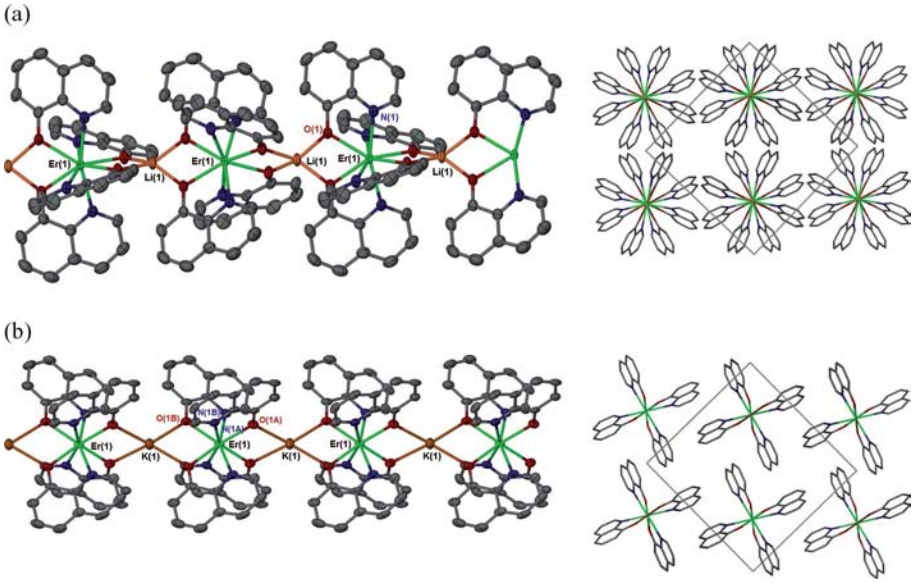

Figure 1. (a) Structure of $[LiEr(OQ)_4]_n$ (**3**) (left), which is representative of $[LiTb(OQ)_4]_n$ (**1**) and $[LiHo(OQ)_4]_n$ (**2**); and (b) the crystal structure of $[KEr(OQ)_4]_n$ (**4**) (left), and their corresponding packing diagrams (right), viewed along the metal–metal axis of the polymeric strands. Clearly visible are the differences in the packing and the symmetry of the crystal structures. $[Ln(OQ)_4]$ units in **4** are eclipsed when viewed along the metal–metal axis (b; right), whereas in **3**, every second $[Ln(OQ)_4]$ unit is rotated by 45° with respect to the preceding one (a; right). All hydrogen atoms have been omitted for clarity.

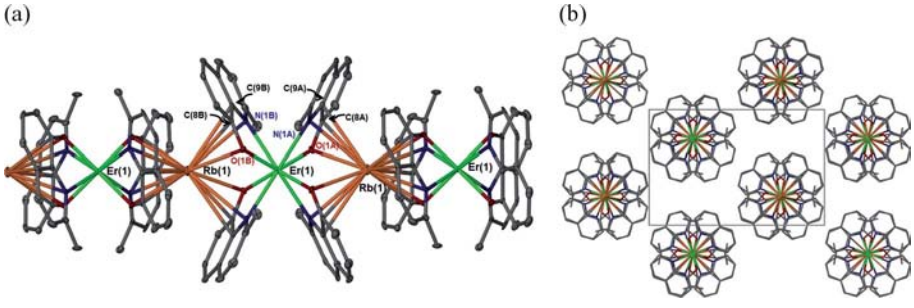

Figure 2. (a) The structure of $[RbEr(MQ)_4]_n$ (**6**), which is representative of $[RbTb(MQ)_4]_n$ (**5**), and (b) the corresponding packing diagram, viewed along the metal–metal axis. All hydrogen atoms have been omitted for clarity.

 © 2011 Wiley-VCH Verlag GmbH & Co. KGaA, Weinheim

metal–metal distances in **1**–**3**, the adjacent $[Ln(OQ)_4]^-$ units adopt a staggered arrangement [Figure 1(a) right]. Li–O bond lengths in **1** and **3** are little affected by the change of the lanthanoid and are 0.57 Å shorter than the corresponding K–O distances in **4**. Relative short K···C distances between K(1) and carbon atoms C(8A) and C(8B) (carbon atoms bound to the oxygen atom) are observed (3.48 and 3.52 Å, respectively), but are near the limit for significant bonding (see below). It appears the steric bulk of the OQ ligands in this case is sufficient to block an increase in the coordination sphere of the four-coordinate potassium metal (cf. Figure 2).

Table 1. Selected bond lengths [Å] in complexes $[AMLn(OQ)_4]_n$ (**1**, **3** and **4**).

	1	**3**		**4**
	Tb	Er		Er
Ln(1)–O(1)	2.341(3)	2.323(2)	Er(1)–O(1A)	2.298(4)
			Er(1)–O(1B)	2.298(4)
Ln(1)–N(1)	2.558(3)	2.521(3)	Er(1)–N(1A)	2.569(4)
			Er(1)–N(1B)	2.545(4)
Li(1)–O(1)	2.005(3)	1.992(2)	K(1)–O(1A)#	2.574(4)
			K(1)–O(1B)	2.566(4)
Li(1)–Ln(1)	3.485(4)	3.470(4)	K(1)–Er(1)	3.972(3)
			K(1)–Er(1)#	3.988(3)

The <Ln–O> bond lengths in **5** and **6** follow the lanthanoid contraction well (Table 2),[26] whereas <Rb–O> distances are unaffected by the change of the lanthanoid metal. The Ln–N distances in **5** and **6** also follow the lanthanoid contraction between eight-coordinate terbium and erbium ($\Delta \approx 0.04$ Å), but the Ln(1)–N(1A/B) and Rb(1)#–N(1A/B) distances in **5** and **6** are unsymmetrical and differ by 0.03 and 0.07 Å, respectively. This leads to unsymmetrical metal–metal distances for Ln(1)–Rb(1) and Ln(1)–Rb(1)#, with a difference of about 0.05 Å in both complexes. The steric effect of the methyl group in the 2-position causes the MQ ligand to rotate resulting in longer M–N and shorter M–O bond lengths when compared with unsubstituted OQ, as has been shown in $[Ln_2AE(Q)_8]$ complexes (AE = Mg, Ca; Q = OQ, MQ).[16] Rb–C distances below 3.50 Å (Table 2) indicate interaction of the ligand π-electron system (see data in ref.[25]) as do close to perpendicular Ln(1)–N(1A/B)–Rb(1) angles in **5** and **6** (Table 2) leading to an overall η^3-N,C,C-binding interaction. A recent survey of the Cambridge Crystallographic Data Centre (CCDC) showed that there are no bridging quinoline μ-N motifs known, but there is precedent for pyridine moieties containing σ–π-arene μ-M–N–M interactions. In the alkali metal coordination compound $\{[Rb_2(\mu_2\text{-phen})_4]I_2\}_n$·MeOH (phen = 1,10-phenanthroline),[27] the phenanthroline ligands bridge (μ_2) through both their nitrogen atoms to form polymeric 1D chains. Close Rb–C distances (≈ 3.5 Å) involving the C atoms of the phen ligand and similar M–N–M angles (≈ 75°) are also observed. When considering all appropriate Rb–C interactions and Rb–N, and regarding the η^3-NCC–Rb unit as occupying two coordination sites, the rubidium ions in **5** and **6** possesses a formal coordination number of twelve, as in the above phen complex.[27] By contrast to the Rb–N interaction, *p*-C–N–Ln angles are near 180°, consistent with a σ-N–Ln interaction. The packing diagram of **6** [Figure 2(b)] also demonstrates the realignment of the MQ ligands, when compared with their OQ analogues (**1**–**4**), to account for the larger ionic radius of rubidium. Unlike the ligands in **1**–**4**, which align parallel to the metal–metal axis, the ligands in **5** and **6** have a non-parallel arrangement.

Table 2. Selected bond lengths [Å] and angles [°] for complexes $[RbLn(MQ)_4]_n$ **5** and **6**.

	5	**6**		**5**	**6**
	Tb	Er		Tb	Er
Ln(1)–O(1A)	2.282(3)	2.243(2)	Rb(1)–C(8B)	3.189(4)	3.152(3)
Ln(1)–O(1B)	2.286(3)	2.240(2)	Rb(1)–C(9B)	3.391(4)	3.400(3)
Rb(1)#–O(1A)	2.942(3)	2.937(2)	Rb(1)#–C(8A)	3.154(4)	3.172(3)
Rb(1)#–O(1B)	2.941(3)	2.936(2)	Rb(1)#–C(9A)	3.423(4)	3.371(3)
Ln(1)–N(1A)	2.730(3)	2.655(3)	Ln(1)–Rb(1)	3.888(1)	3.895(1)
Ln(1)–N(1B)	2.696(3)	2.688(3)	Ln(1)–Rb(1)#	3.947(1)	3.841(1)
Rb(1)#–N(1A)	3.468(3)	3.367(3)	Ln(1)–N(1A)–Rb(1)	78.10(8)	78.26(7)
Rb(1)#–N(1B)	3.389(3)	3.435(3)	Ln(1)–N(1B)–Rb(1)	78.53(8)	77.94(7)

The packing of the crystal structures affects intermolecular interactions. Weak offset π-π face-to-face interactions can be found in **1**, **3** and **4**. The mean planes of ligand A and its symmetry-related counterpart are parallel, as dictated by symmetry, at a distance of 3.49 Å (in **1** and **3**) and 3.45 Å in **4**. Also in **4**, a CH···π edge-to-face interaction is observed between H(5A) (a hydrogen atom in a calculated position) and C(9B)#. They are 2.68 Å apart. The canals that run along the *c*-axis in **1** and **3** are approximately 4.5 Å in diameter and thus too small to fit the flux molecules used in the syntheses (i.e., TMB). The tilting of the MQ ligands towards the metal–metal axis in **4** prevents analogous canals being observed. Crystallographic and refinement data for **1**, **3** and **4** are in Table 3 and for **5** and **6** in Table 5.

The novel homometallic dimeric caesium derivative $[Cs_2(\mu\text{-}MQ)_2(HMQ)_2]$ (**7**) (Figure 3), the product of the elevated temperature reaction between Cs(MQ) and $Er(MQ)_3$ in TMB, comprises one unique caesium atom, one unique deprotonated chelating bridging 8-quinaldinolate (MQ) ligand and one unique chelating bridging neutral terminal 8-hydroxyquinaldine (HMQ) ligand in the asymmetric unit. Dimerisation occurs through the deprotonated bridging MQ ligand (and its symmetry equivalent) by both its oxygen and nitrogen donor atoms. Two additional methyl-carbon/methyl-hydrogen–Cs interactions saturate the coordination sphere.

The centrosymmetric structure (its inversion centre is situated halfway along the Cs–Cs vector) exhibits asymmetric Cs–N bonding of the chelating-bridging ligand B. The difference is a large 0.345 Å between Cs(1)–N(1B) and Cs(1)–N(1B)# [3.561(2) and 3.216(3) Å, respectively] (Table 4). Bond lengths and angles do not suggest a simple division into σ and π interactions. For comparison, the Cs(1)–N(1A) distance of the terminal ligand is 3.111(3) Å. The <Cs–N> distances fall within the range of earlier reported structures, see, for example, the pyridine-bridged $[Cs\{P(H)tBu_3$-

 © 2011 Wiley-VCH Verlag GmbH & Co. KGaA, Weinheim

Table 3. Crystallographic data for complexes **1**, **3** and **4**.

	1	**3**	**4**
Chemical formula	$C_{36}H_{24}LiN_4O_4Tb$	$C_{36}H_{24}ErLiN_4O_4$	$C_{36}H_{24}ErKN_4O_4$
Formula mass	742.45	750.79	782.95
Crystal system	tetragonal	tetragonal	monoclinic
Space group	*P*4/*ncc*	*P*4/*ncc*	*P*2/*n*
a [Å]	14.6097(2)	14.6496(2)	13.578(6)
b [Å]	14.6097(2)	14.6496(2)	7.960(4)
c [Å]	13.9396(2)	13.8779(2)	14.258(7)
β [°]	90	90	90.343(19)
Unit cell volume [Å^3]	2975.31(7)	2978.35(7)	1541.0(13)
Temperature [K]	123(1)	293(1)	123(1)
Z	4	4	2
Absorption coefficient [mm^{-1}]	2.425	2.866	2.906
No. of reflections measured	24325	34730	6335
No. of independent reflections	1717	1714	2944
R_{int}	0.0557	0.0328	0.0421
Final R_1 values [$I > 2\sigma(I)$]	0.0279	0.0245	0.0377
Final $wR(F^2)$ values [$I > 2\sigma(I)$]	0.0521	0.0464	0.0799
Final R_1 values (all data)	0.0636	0.0372	0.0480
Final $wR(F^2)$ values (all data)	0.0654	0.0544	0.0866
Goodness of fit on F^2	1.127	1.130	1.028

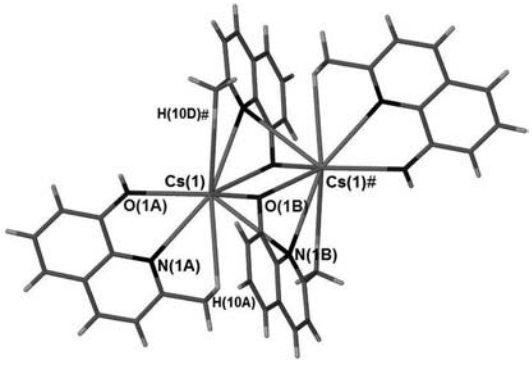

Figure 3. Molecular structure of $[Cs_2(MQ)_2(HMQ)_2]$ (7). # indicates symmetry operation: *1* –*x*, –*y*, –*z*.

$C_6H_2\}_2(\mu\text{-py})]_n$ [P(H)*t*Bu$_3$C$_6$H$_2$ = 2,4,6-tri-*tert*-butylphenylphosphide][28] in which the Cs–N distances are 3.375(10) Å. Unlike the disparate bridging Cs–N bond lengths in **7**, <Cs–O> bond lengths involving chelating-bridging ligand B are symmetrical (av. 3.079 Å). The terminal Cs(1)–O(1A) bond length is 0.051 Å shorter than the bridging Cs–O distances, despite the charge difference between MQ and HMQ.

Table 4. Selected bond lengths [Å] and angles [°] for complex **7**.

$[Cs_2(MQ)_2(HMQ)_2]$			
Cs(1)–O(1A)	3.028(2)	Cs(1)–N(1A)	3.111(3)
Cs(1)–O(1B)	3.080(2)	Cs(1)–N(1B)	3.561(2)
Cs(1)–O(1B)#	3.078(2)	Cs(1)–N(1B)#	3.216(3)
H(1)–O(1B)#	1.63(4)	Cs(1)–C(10A)	3.789(4)
Cs(1)–C(8B)	3.766(3)	Cs(1)–C(10B)#	4.035(4)
Cs(1)–H(10A)	3.24	Cs(1)–H(10D)#	3.25
Cs(1)–Cs(1)#	3.993(1)		
H(10A)–Cs(1)–H(10D)#		144.46	
Cs(1)–N(1B)–Cs(1)#		72.01(5)	

Distances of 3.24 and 3.25 Å between Cs(1) and H(10A) and H(10D)#, respectively (hydrogen atoms in calculated positions), strongly suggest an interaction. The corresponding methyl-carbon Cs(1)–C(10A/B) distances are 3.789(4) and 4.035(4) Å, which fall near the range of Cs–C bond lengths in the literature. A survey of the CCDC showed that reported Cs–C values range between 3.198 to 3.921 Å.[25] In the 1D polymeric $[Cs(C_6H_2tBu_3\text{-}2,4,6)(dme)]_n$[29] there is an agostic C–Cs interaction from one of the methyl-carbon atoms of the *t*Bu-groups (3.596 Å), and in the dimeric borane-stabilised phosphane carbanion $[Cs\{(Me_3Si)_2\{Me_2P(BH_3)\}C\}pmdta]_2$[30] (pmdta = pentamethyldiethylentriamine), the caesium pmdta-methyl carbon agostic bond lengths range from 3.629(6)–3.881(5) Å. Thus, in the present case, one methyl-carbon–Cs interaction falls within this range whilst the other is slightly longer. The apparent naked face of the caesium cation (Figure 3) is occupied by neighbouring dimers, blocking access to the coordination sphere. If each C(H)–Cs interaction is viewed as occupying a single coordination site, the overall coordination number is eight.

The dimeric complexes are connected in a 1D-chain polymeric network along the crystallographic *b*-axis through very strong hydrogen bonds (hydrogen atoms were located on the difference map) between phenolic H(1) and the adjacent phenolate oxygen O(1B)#; the distance is only 1.63 Å (Figure 4). The angle between donor and acceptor

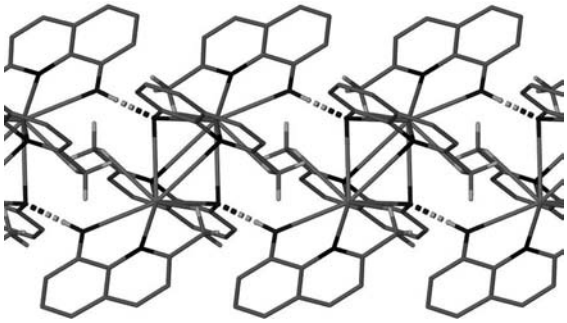

Figure 4. Hydrogen bonding network in $[Cs_2(MQ)_2(HMQ)_2]$ (**7**). All hydrogen atoms except methyl group hydrogen atoms and hydrogen atoms involved in hydrogen bonding have been omitted for clarity. Hydrogen bonds are depicted as dashed lines.

 © 2011 Wiley-VCH Verlag GmbH & Co. KGaA, Weinheim

Table 5. Crystallographic data for complexes **5**–**7**.

	5	**6**	**7**
Chemical formula	$C_{40}H_{32}N_4O_4RbTb$	$C_{40}H_{32}ErN_4O_4Rb$	$C_{40}H_{34}Cs_2N_4O_4$
Formula mass	877.09	885.43	900.53
Crystal system	orthorhombic	orthorhombic	monoclinic
Space group	*Pccn*	*Pccn*	$P2_1/n$
a [Å]	18.610(4)	18.641(4)	14.6325(4)
b [Å]	12.250(3)	12.191(2)	7.3252(2)
c [Å]	15.670(3)	15.471(3)	16.7831(5)
β [°]	90	90	96.642(1)
Unit cell volume [Å^3]	3572.3(12)	3515.8(12)	1786.84(9)
Temperature [K]	100(2)	100(2)	123(1)
Z	4	4	2
Absorption coefficient [mm^{-1}]	3.380	3.810	2.087
No. of reflections measured	34554	36310	11644
No. of independent reflections	2851	2773	3978
R_{int}	0.1301	0.0445	0.0443
Final R_1 values [$I > 2\sigma(I)$]	0.0429	0.0332	0.0323
Final $wR(F^2)$ values [$I > 2\sigma(I)$]	0.1148	0.0924	0.0624
Final R_1 values (all data)	0.0517	0.0371	0.0459
Final $wR(F^2)$ values (all data)	0.1220	0.0955	0.0678
Goodness of fit on F^2	1.052	1.110	1.040

atoms is very close to the ideal 180°. Crystallographic and refinement data for **7** are given in Table 5.

$[KYb_2(MQ)_7]$ (**8**) is very different from the polymeric Ln/Group I heterobimetallics (**1**–**6**) presented above and has a much more complex binding pattern of the MQ ligands. Complex **8** is a monomeric trinuclear complex (space group $P2_1/c$), in which the three metal atoms are arranged triangularly. Eight-coordinate Yb(1) and seven-coordinate Yb(2) each are ligated by one terminal N,O chelating MQ ligand (ligands A and C, respectively) and one chelating bridging ligand (B) that connects these two metals together, N(1B) being bound to Yb(1). Chelating bridging ligands (D and F) are κ^1(N)-μ-κ^1:κ^1(O) bonded to the potassium metal and Yb(2) and Yb(1), respectively. Two κ^1(N)-μ_3-κ^1:κ^1:κ^1(O) ligands (E and G) are attached to all of Yb(1), Yb(2) and K(1) through O(1E) or O(1G) with N(1E) and N(1G) bound to Yb(2) and Yb(1), respectively. The coordination environments of Yb(1) and Yb(2) are similar but ligand B, the sole ligand to bridge only Yb(1,2), coordinates through its nitrogen atom to Yb(1), but not to Yb(2). In summary, there are two terminal chelating ligands, three that bridge two metals and two that bridge all metals. Yb(1) is coordinated by O(1A,B,E,F,G) and N(1A,B,G), Yb(2) by O(1B,C,D,E,G) and N(1C,E), and K(1) by O(1D,E,F,G) and N(1D,F).

Generally, the average M–O bond length increases in the sequence terminal M–O(κ^1) < bridging bidentate M–O(κ^1:κ^1) < bridging tridentate M–O(κ^1:κ^1:κ^1) demonstrating the use of one, two and three electron lone pairs in bonding (Table 6). Eight-coordinate Yb(1)–O distances follow this sequence strictly. They increase from 2.183(6) Å for terminal Yb(1)–O(1A) over 2.354(6) Å for bridging Yb(1)–O(1B) to 2.451(6) Å for tridentate bridging Yb(1)–O(1E), an increase of 0.268 Å (Table 6). This increase is less for bridging bidentate Yb(1)–O(1F) [2.198(6) Å] and bridging tridentate Yb(1)–O(1G) [2.274(6) Å], an overall increase of only 0.091 Å. The Yb(1)–O(1F) distance is effectively the same as for the terminal Yb(1)–O(1A) [2.183(6) Å] (allowing for 3 e.s.d.). The disparity in bond lengths between Yb(1)–(O1B) and Yb(1)–(O1F) can be explained by the charge size effect of Yb(2) and potassium, respectively, as the other bridging atom. In the case of ligands (E,G), in which oxygen is bound to all three metals, the former has a much longer bond to eight coordinate Yb(1) (ca. 0.15 Å) whilst the latter has a long Yb(1)–N(1G) bond. Cumulative bond length differences show that Yb–O and Yb–N distances are 0.05 and 0.11 Å longer for Yb(1), respectively, than for Yb(2), compared with 0.06 Å difference in ionic radii between seven- and eight-coordinate Yb^{3+}.[26] The steric effect of the 2-methyl group is more pronounced on the Yb–N bond length with the higher coordination number Yb atom.

Table 6. Selected bond lengths [Å] for complex **8**.

$[Yb_2K(MQ)_7]$					
Terminal		Bridging			
		μ-κ^1:κ^1(O)		μ_3-κ^1:κ^1:κ^1(O)	
Yb(1)–O(1A)	2.183(6)	Yb(1)–O(1B)	2.354(6)	Yb(1)–O(1E)	2.451(6)
Yb(2)–O(1C)	2.165(6)	Yb(1)–O(1F)	2.198(6)	Yb(1)–O(1G)	2.274(6)
		Yb(2)–O(1B)	2.298(6)	Yb(2)–O(1E)	2.287(6)
Yb(1)–N(1A)	2.577(7)	Yb(2)–O(1D)	2.167(6)	Yb(2)–O(1G)	2.298(5)
Yb(2)–N(1C)	2.507(7)	K(1)–O(1D)	2.701(6)	K(1)–O(1E)	2.811(6)
		K(1)–O(1F)	2.740(7)	K(1)–O(1G)	2.942(6)
		Yb(1)–N(1B)	2.576(7)	Yb(1)–N(1G)	2.668(7)
		K(1)–N(1D)	2.750(8)	Yb(2)–N(1E)	2.478(7)
		K(1)–N(1F)	2.726(8)		
Yb(1)–Yb(2)	3.491(2)	K(1)–C(7E)	3.468(10)	K(1)–C(8D)	3.448(10)
Yb(1)–K(1)	3.724(3)	K(1)–C(8E)	3.064(9)	K(1)–C(9D)	3.486(10)
Yb(2)–K(1)	3.662(3)	K(1)–C(8G)	3.222(8)	K(1)–C(8F)	3.527(10)

The much larger ionic radius of the potassium metal compared with the ytterbium metals [1.38 Å for K^+ (CN = 6) compared with 0.92 and 0.98 Å for Yb^{3+} (CN = 7 and 8, respectively)],[26] leads to longer <K–O> and <K–N> bond lengths. Similar observations made for the Yb–O

 © 2011 Wiley-VCH Verlag GmbH & Co. KGaA, Weinheim

bond lengths can be made for the corresponding K–O distances in that <K–O> bond lengths involving μ-κ^1:κ^1(O) oxygen atoms are 0.15 Å shorter than the respective <K–O> distances involving tridentate μ$_3$-κ^1:κ^1:κ^1(O) oxygen atoms (2.72 and 2.87 Å, respectively). The longer bond lengths involving the potassium atom are also reflected in unequal metal–metal bond lengths [K(1)–Yb(1,2) ca. 0.2 Å longer than Yb(1)–Yb(2)] distorting the trimetallic triangle from equilateral. Donation of π-electron density from MQ ligands to the coordinatively unsaturated potassium metal is achieved by the tilting of the ligands resulting in short distances between the potassium metal and various carbon atoms of the MQ ligands (Table 6). They mainly involve *ipso* carbon atoms and in two cases also an adjacent carbon atom (Figure 5 shows some as bonds). These contacts provide a coordination number for potassium higher than six and demonstrate the response of the structure to compensate for the otherwise coordinatively unsaturated potassium. Similar K–C bond lengths (3.09–3.41 Å) have been reported for [K(PhMe)(Ln(*t*Bu$_2$pz)$_4$)]·2PhMe.[24] In addition, interaction distances between the *ipso* carbon atoms of the aryloxide and potassium in [KY(OAr)$_4$(thf)$_5$][31] (OAr = 2,6-dimethylphenolate; thf = tetrahydrofuran) range between 3.288(9)–3.400(10) Å, similar to the analogous K[Nd(Odip)$_4$][32] (Odip = 2,6-bis(isopropyl)phenolate) [3.256(9) Å] and [KSm(OAr′)$_3$]$_n$[33] (OAr′ = 2,6-di-*tert*-butyl-4-methylphenolate) [3.310(10) and 3.534(13) Å]. Crystallographic and refinement data for **8** are given in Table 8.

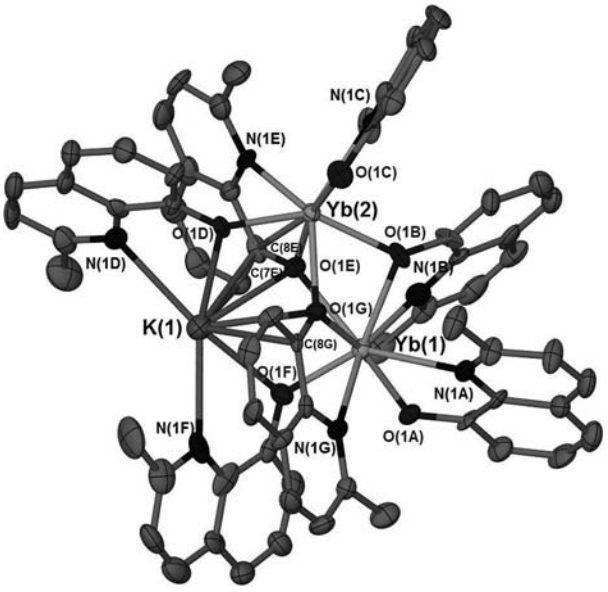

Figure 5. Molecular structure of [KYb$_2$(MQ)$_7$] (**8**). All hydrogen have been atoms omitted for clarity. Thermal ellipsoids are set at 50% probability.

Spontaneous crystallisation from a supersaturated solution of HOQ and NaOH in ethanol led to the isolation of the 2D sheet polymer [Na$_4$(OQ)$_4$(H$_2$O)$_8$]$_n$ (**9**). The two crystallographically unique sodium atoms are each surrounded by one chelating (N, O) OQ ligand and four water molecules in a distorted octahedral fashion. All four water molecules bridge to adjacent sodium ions to form a double-stranded polymer, which propagates on the *ab*-plane (Figure 6). Within each layer, an extensive hydrogen-bonding network holds the structure together (see Table 7 for bond lengths; crystal and refinement data are given in Table 8).

Table 7. Selected bond lengths [Å] for complex **9**.

[Na$_4$(OQ)$_4$(H$_2$O)$_8$]$_n$			
Na(1)–N(1)	2.420(5)	Na(2)–N(2)	2.434(5)
Na(1)–O(1)	2.396(5)	Na(2)–O(3)	2.437(6)
Na(1)–O(2)	2.450(5)	Na(2)–O(4)#	2.782(6)
Na(1)–O(2)#	2.450(5)	Na(2)–O(5)	2.408(5)
Na(1)–O(3)	2.461(6)	Na(2)–O(6)	2.403(5)
Na(1)–O(4)	2.538(6)	Na(2)–O(6)#	2.448(5)
H-bonds			
H(2B)–O(1)#	1.74(2)	H(4A)–O(3)#	1.88(4)
H(6B)–O(1)	1.91(3)	H(6A)–O(5)#	1.92(3)
		H(3B)–O(5)#	1.71(2)

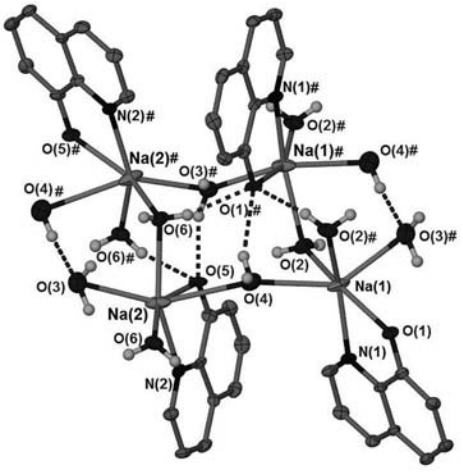

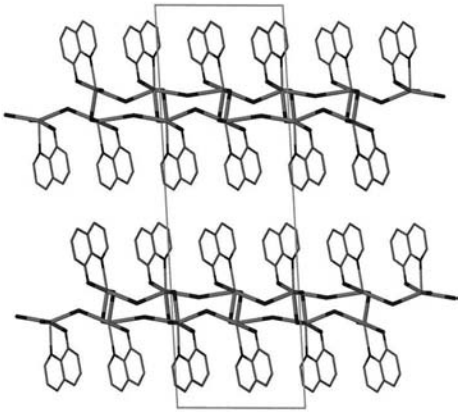

Figure 6. Molecular structure of [Na$_4$(OQ)$_4$(H$_2$O)$_8$]$_n$ (**9**), left, and packing diagram viewed along the *b*-axis displaying the sheet structure, right. Thermal ellipsoids set at 50% probability. Dashed lines indicate the hydrogen-bonding network. OQ hydrogen atoms have been omitted for clarity.

 © 2011 Wiley-VCH Verlag GmbH & Co. KGaA, Weinheim

Table 8. Crystallographic data for complexes **8**–**10**.

	8	**9**	**10**
Chemical formula	$C_{70}H_{56}KN_7O_7Yb_2$	$C_{18}H_{20}N_2Na_2O_6$	C_9H_8ClNO
Formula mass	1492.40	406.34	181.61
Crystal system	monoclinic	monoclinic	triclinic
Space group	$P2_1/c$	$P2_1/c$	$P\bar{1}$
a [Å]	17.967(4)	9.6338(19)	6.9164(3)
b [Å]	15.412(3)	6.2708(13)	7.7424(3)
c [Å]	22.955(5)	30.289(6)	9.2156(4)
α [°]	90	90	98.8350(10)
β [°]	110.22(3)	93.42(3)	111.2690(10)
γ [°]	90	90	108.3590(10)
Unit cell volume [Å^3]	5965(2)	1826.6(6)	415.98(3)
Temperature [K]	173(2)	123(1)	123(1)
Z	4	4	2
Absorption coefficient [mm^{-1}]	3.249	0.150	0.403
No. of reflections measured	61011	9134	3116
No. of independent reflections	13678	4115	1809
R_{int}	0.2152	0.0772	0.0156
Final R_1 values [$I > 2\sigma(I)$]	0.0660	0.1154	0.0292
Final $wR(F^2)$ values [$I > 2\sigma(I)$]	0.1136	0.2427	0.0769
Final R_1 values (all data)	0.1806	0.1823	0.0316
Final $wR(F^2)$ values (all data)	0.1486	0.2708	0.0787
Goodness of fit on F^2	0.994	1.067	1.044

In an attempt to synthesise homoleptic K(OQ) utilising 1,2,3,4-tetrachlorobenzene as a flux instead of the normally employed TMB, a few single crystals of 8-hydroxyquinolinium chloride (**10**) were isolated. The quinolinium and hydroxy hydrogen atoms were located on the difference map. Compound **10** crystallises as a hydrogen-bonded step-shaped dimer in which both the hydroxy and the quinolinium hydrogen atoms bind to a near chlorine atom (Figure 7); the H···Cl distances are 2.08(3) and 2.27(2) Å, respectively. Crystal packing shows intermolecular offset π-π face-to-face interactions in a sheet arrangement of the OQ molecules, the sheets being 3.30 Å apart.

To the best of our knowledge, this is the first hydroxyquinolinium structure involving the unsubstituted OQ ligand without the inclusion of lattice solvent. Previously, many quinolinium structures (including Q derivatives) included lattice molecules or ions such as water[34] or nitrate.[35]

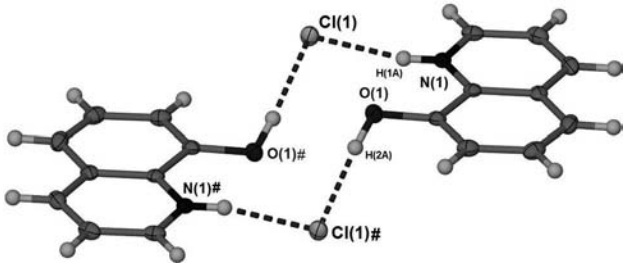

Figure 7. Molecular structure of the hydrogen-bonded 8-hydroxyquinolinium chloride dimer (**10**). Thermal ellipsoids are set at 50% probability. Dashed lines indicate hydrogen bonding.

Conclusion

The polymeric lanthanoid alkali $[AMLn(Q)_4]_n$ [Q = OQ: AM = Li, Ln = Tb (**1**), Ho (**2**), Er (**3**); AM = K, Ln = Er (**4**); Ln = MQ: AM = Rb, Ln = Tb (**5**), Er (**6**)] complexes, which were isolated from reactions between AMQ and $Ln(Q)_3$ in an inert flux at elevated temperatures, demonstrate the versatility of the pseudo-solid-state approach for the synthesis of novel lanthanoid metal–organic compounds. From an attempt to synthesise $[CsEr(MQ)_4]_n$, the homometallic, dimeric complex $[Cs_2(MQ)_2(HMQ)_2]$ (**7**) was isolated. The compounds **4**–**7** represent the first examples of *homo*- and heterobimetallic lanthanoid OQ/MQ complexes involving alkali metals heavier than lithium. Previously, only $[Li_6(OQ)_6]$[18a] and $[Li_6(MQ)_6]$[18b] were known and some sodium and potassium complexes of Q derivatives (introduction). A sealed-tube reaction between $Yb(MQ)_3$ and $K_2C_2O_4$ yielded the structurally novel heterobimetallic $[KYb_2(MQ)_7]$ (**8**) complex. It represents the first example of a monomeric heterobimetallic homoleptic MQ complex-comprising an alkali metal, a departure from the polymeric alkali metal lanthanoid complexes **1**–**6**. The crystallisation of a simple but previously elusive hydrated sodium 8-quinolinolate complex (**9**) was also achieved.

Experimental Section

The precursor metal 8-quinolinolate and 8-quinaldinolate complexes were prepared by mixing aqueous solutions of the metal chloride (either as purchased or from dissolution of the metal oxide in hydrochloric acid) and a stoichiometric amount of Na(OQ) or Na(MQ) (prepared by a stoichiometric reaction of HOQ/HMQ with NaOH in EtOH and subsequent concentration of the solution). The precipitated product was filtered and dried. Alterna-

 © 2011 Wiley-VCH Verlag GmbH & Co. KGaA, Weinheim

tively, MQ precursors were also prepared by treatment of the same aqueous Ln^{3+} solution (pH ≈ 5) with a stoichiometric amount of an ethanolic solution of HMQ and NH_3 (molar ratio 1:1), followed by filtration, washing and drying of the precipitated complex. IR spectra were obtained with a Perkin–Elmer Spectrum RX1 spectrometer and with a Specac ATR with a diamond anvil linked to a Bruker Equinox 55a spectrometer fitted with an MCT detector. Powder XRD experiments were conducted using a Bruker AXS D8 and a Philips 1140 diffractometer with a Cu anode at λ = 1.5418 Å and a graphite monochromator. Powdered samples were thoroughly ground in an agate mortar prior to measurement. Microanalyses were carried out by the Campbell Microanalytical Laboratory, University of Otago, NZ.

General Procedure: Reactions were performed by heating the finely ground reaction mixture (ca. 0.50 g) with the desired stoichiometry of the reactants and a flux [1,2,4,5-tetramethylbenzene (TMB)] (1.5 g) in a sealed and evacuated thick-walled glass tube at 210 or 270 °C for several days. After visual examination confirmed that a reaction had occurred, the flux was removed from the reaction mixture by sublimation in an open-end oven at 150 °C for 2–4 h. The cooled tubes were opened in air and crystalline material was handpicked from the bulk residual powder and characterised by single-crystal X-ray crystallography. For compounds **1**, **5**–**7**, samples of crystals in viscous hydrocarbon oil, following selection of crystals for X-ray examination, were manually separated from powders, worked with hexane to remove the oil, dried and sent for elemental analysis.

$[Li_6(OQ)_6]$: $Eu(OQ)_3$ (0.15 g, 0.26 mmol), LiOQ (0.15 g, 0.99 mmol) and TMB (1.00 g, 7.45 mmol) were initially heated to 120 °C for 14 d and then the temperature was increased to 210 °C and held for 21 d. Yellow crystals of the title complex were handpicked from the bulk powder and were identified by comparison of the unit cell with that reported in the literature.[18a] Crystal yield: 0.003 g; 1.5%.

$[LiTb(OQ)_4]_n$ (1): $Tb(OQ)_3$ (0.15 g, 0.25 mmol), LiOQ (0.15 g, 0.99 mmol) and TMB (1.50 g, 11.10 mmol) were heated to 270 °C for 42 d. Yellow crystals of the title complex were handpicked from the bulk powder. Crystal yield: 0.018 g; 10%. M.p.: > 360 °C. IR (as Nujol mull): $\tilde{\nu}$ = 1569 (m), 1498 (m), 1463 (s), 1377 (s), 1322 (m), 1281 (w), 1226 (w), 1107 (m), 1033 (w), 823 (m), 728 (m) cm^{-1}. Powder XRD data on bulk powder [*d* spacing (Å), rel. int.]: *10.39* (100); *9.76* (20); *7.05* (24); *6.30* (17); *5.79* (30); *5.21* (15); *4.66* (42); *4.41* (59); *4.17* (34); *3.87* (21); *3.46* (16); *3.28* (20); *2.98* (16), corresponded well with that calculated from single-crystal data, showing only minor contamination by an unidentified crystalline material.

$[LiHo(OQ)_4]_n$ (2): $Ho(OQ)_3$ (0.15 g, 0.25 mmol), LiOQ (0.15 g, 0.99 mmol) and TMB (1.50 g, 11.10 mmol) were heated to 270 °C for 35 d. Very few yellow crystals of the title complex (as identified by unit-cell comparison with complexes **1** and **3**) were handpicked from the bulk powder. Crystal yield: 0.022 g; 12%. M.p.(dec.): 320 °C. IR (as Nujol mull): $\tilde{\nu}$ = 1570 (w), 1499 (m), 1464 (s), 1377 (s), 1323 (m), 1281 (w), 1233 (w), 1109 (m), 1034 (w), 823 (w), 791 (w), 754 (w), 729 (m) cm^{-1}. Powder XRD data on bulk powder [*d* spacing (Å), rel. int.]: *10.46* (100); *7.37* (4); *7.05* (4); *6.34* (2); *5.82* (9); *5.20* (5); *4.66* (19); *4.41* (26); *4.18* (9); *3.88* (5); *3.46* (6); *3.28* (8); *2.97* (6); *2.88* (4), indicated the presence of the title complex in the weakly diffracting powder (when compared with the calculated powder XRD pattern from complex **3**). $C_{36}H_{24}HoLiN_4O_4$ (748.48): calcd. C 58.18, H 3.23, N 7.54; found C 58.92, H 3.29, N 7.52.

$[LiEr(OQ)_4]_n$ (3): $Er(OQ)_3$ (0.15 g, 0.25 mmol), LiOQ (0.15 g, 0.99 mmol) and TMB (1.00 g, 7.45 mmol) were initially heated to 150 °C for 14 d. The temperature was then increased to 210 °C for 35 d. Yellow crystals of the title complex were handpicked from the bulk powder. Crystal yield: 0.013 g; 7%. M.p. (dec.): 330 °C. IR (as Nujol mull): $\tilde{\nu}$ = 1570 (m), 1499 (m), 1465 (s), 1376 (s), 1323 (m), 1281 (m), 1233 (w), 1109 (m), 823 (m), 791 (m), 729 (m) cm^{-1}. Powder XRD data on bulk powder [*d* spacing (Å), rel. int.]: *10.46* (100); *6.99* (13); *6.32* (6); *5.79* (17); *4.66* (22); *4.41* (26); *4.17* (13); *3.87* (10); *3.46* (8); *3.29* (11); *2.98* (8), corresponded well with that calculated from single-crystal X-ray data, showing only minor contamination by an unidentified crystalline material.

$[KEr(OQ)_4]_n$ (4): $Er(OQ)_3$ (0.15 g, 0.25 mmol), KOQ (0.15 g, 0.82 mmol) and TMB (1.50 g, 11.10 mmol) were heated to 270 °C for 42 d. Yellow crystals of the title complex were handpicked from the bulk powder. Crystal yield: 0.015 g; 8%. M.p.: > 300 °C. IR (as Nujol mull): $\tilde{\nu}$ = 1567 (w), 1493 (m), 1461 (s), 1377 (s), 1322 (m), 1280 (w), 1170 (w), 1106 (m), 821 (w), 803 (w 786w), 727 (m) cm^{-1}. Powder XRD data on bulk powder [*d* spacing (Å), rel. int.]: *9.87* (77); *7.79* (57); *7.25* (12); *6.91* (19); *6.19* (16); *4.94* (15); *4.48* (43); *4.33* (34); *3.81* (14); *3.16* (16); *2.87* (13), corresponded well with that calculated from single-crystal X-ray data.

$[RbTb(MQ)_4]_n$ (5): $Tb(MQ)_3$ (0.30 g, 0.47 mmol), RbMQ (0.20 g, 0.82 mmol) and TMB (1.50 g, 11.17 mmol) were heated to 210 °C and kept at that temperature for 9 d. Red crystals of $[RbTb(MQ)_4]_n$ were handpicked from the charred bulk powder, which was not further characterised. Crystal yield: 0.010 g; 3%. IR: $\tilde{\nu}$ = 3030 (m), 1591 (w), 1555 (s), 1501 (m), 1426 (s), 1368 (m), 1330 (s), 1275 (s), 1096 (m), 825 (m), 733 (m) cm^{-1}. $C_{40}H_{32}N_4O_4RbTb$ (877.11): calcd. C 54.77, H 3.67, N 6.38; found C 55.04, H 3.61, N 6.42.

$[RbEr(MQ)_4]_n$ (6): $Er(MQ)_3$ (0.15 g, 0.23 mmol), RbMQ (0.20 g, 0.82 mmol) and TMB (1.50 g, 11.17 mmol) were heated to 210 °C and kept at that temperature for 9 d. Red crystals of $[RbEr(MQ)_4]_n$ were handpicked from the charred bulk powder, which was not further characterised. Crystal yield: 0.012 g; 5%. IR: $\tilde{\nu}$ = 3035 (m), 1608 (w), 1587 (m), 1499 (m), 1425 (s), 1368 (m), 1329 (s), 1234 (s), 1098 (m), 825 (m), 734 (m) cm^{-1}. $C_{40}H_{32}ErN_4O_4Rb$ (885.45): calcd. C 54.26, H 3.64, N 6.32; found C 54.53, H 3.03, N 5.15.

$[Cs_2(MQ)_2(HMQ)_2]$ (7): $Er(MQ)_3$ (0.31 g, 0.23 mmol), CsMQ (0.16 g, 0.54 mmol) and TMB (1.50 g, 11.17 mmol) were heated to 210 °C and kept at that temperature for 6 d. Orange crystals of $[Cs_2(MQ)_2(HMQ)_2]$ were handpicked from the charred bulk powder, which was not further characterised. Crystal yield: 0.014 g; 7%. IR: $\tilde{\nu}$ = 3368 (br), 3035 (s), 1586 (s), 1499 (m), 1426 (s), 1367 (m), 1330 (s), 1278 (s), 1098 (m), 826 (m), 737 (s) cm^{-1}. $C_{40}H_{34}Cs_2N_4O_4$ (900.55): calcd. C 53.35, H 3.80, N 6.33; found C 54.81, H 3.13, N 5.23.

$[Yb_2K(MQ)_7]$ (8): $Yb(MQ)_3$ (0.30 g, 0.46 mmol), $K_2C_2O_4{\cdot}H_2O$ (0.2 g, 1.08 mmol) and TMB (1.50 g, 11.17 mmol) were heated to 270 °C and kept at that temperature for 16 d. Yellow crystals of $[Yb_2K(MQ)_7]$ were handpicked from the bulk powder. Crystal yield: 0.012 g; 6%. IR: $\tilde{\nu}$ = 3035 (m), 1559 (s), 1502 (m), 1456 (s), 1427 (s), 1371 (m), 1324 (m), 1301 (m), 1238 (s), 1099 (s), 827 (m), 737 (s) cm^{-1}. Powder XRD data on bulk powder [*d* spacing (Å), rel. int.]: *12.52* (27); *11.67* (41); *10.45* (29); *9.07* (43); *8.33* (30); *4.97* (37); *4.53* (25); *4.35* (24); *4.08* (31); *3.10* (51); *2.97* (60); *2.82* (94); *2.76* (41); *2.62* (47); *2.51* (42); *2.46* (100); *2.27* (27); *2.08* (29); *1.81* (24), showing the presence of the title complex and of $K_2C_2O_4{\cdot}H_2O$.

$Yb(MQ)_3$ and $CaCO_3$: $Yb(MQ)_3$ (0.30 g, 0.46 mmol), $CaCO_3$ (0.10 g, 1.00 mmol) and TMB (1.50 g, 11.17 mmol) were heated to 270 °C and kept at that temperature for 16 d. Pale yellow crystals of HMQ could be handpicked from the bulk powder. [*d* spacing

 © 2011 Wiley-VCH Verlag GmbH & Co. KGaA, Weinheim

[Å], rel. int.]: *13.08* (100); *12.19* (52); *9.42* (67); *8.25* (52); *7.13* (24); *6.86* (32); *4.20* (28); *3.41* (48); *3.29* (38); *3.12* (27); *3.05* (50); *2.71* (32); *2.49* (35); *2.38* (30); *2.34* (29); *1.98* (32); *1.88* (28), resembled that of $[Er_3(MQ)_7CO_3]$[16] inferring formation of isostructural $[Yb_3(MQ)_7CO_3]$ and it also showed lines of unreacted $CaCO_3$.

$[Na_4(OQ)_4(H_2O)_8]_n$ (9): The combined yellow solution of 8-hydroxyquinoline (9.07 g; 62.5 mmol) and NaOH (2.50 g; 62.5 mmol) in ethanol was evaporated upon which yellow crystals of the title complex formed. Yield: 9.39 g; 90%. M.p. (dec.): 290 °C. IR (as Nujol mull): $\tilde{\nu}$ = 3362 (br), 1718 (w), 1563 (s), 1495 (s), 1327 (s), 1227 (m), 1171 (m), 1101 (s), 1033 (w), 969 (w), 844 (m), 818 (m), 780 (m), 731 (m), 714 (m), 654 (w) cm^{-1}. $C_{18}H_{20}N_2Na_2O_6$ (406.35): calcd. C 53.20, H 4.96, N 6.89; found C 53.13, H 4.94, N 6.78.

8-Hydroxyquinolinium Chloride (10): K(OQ) (0.38 g, 2.07 mmol) and 1,2,3,4-tetrachlorobenzene (1.00 g, 4.63 mmol) were heated to 210 °C and kept at that temperature for 49 d. Crystals of the title complex were handpicked from the blackened bulk powder. Crystal yield (estimated): 0.005 g; 1.3%.

Crystallography: Low-temperature single-crystal X-ray diffraction experiments were performed with a Bruker Apex II KAPPA CCD (**1**, **3**, **4**, **7**, **9**, **10**) or an Enraf Nonius Kappa CCD (**8**) with Mo-K_α radiation (λ = 0.71073 Å) and equipped with an Oxford Instruments nitrogen gas cryostream. Measurements for **5** and **6** were made on the MX1 beam-line at the *Australian Synchrotron*. The beamline operated at ≈ 1.60 keV (λ = 0.77369 Å). Single crystals were mounted on a glass fibre in viscous hydrocarbon oil. Crystals were quench-cooled to 123(2) K (**3**, **4**, **7**, **9**, **10**), 173(2) K (**8**) or 100(2) K (**5** and **6**). Analysis of diffraction data collected with the Bruker Apex II KAPPA CCD was performed by using SAINT+ within the APEX2[36] software package. Empirical absorption corrections were applied to all data by using SADABS.[37] Analysis of diffraction data collected with the Enraf Nonius Kappa CCD was performed by using DENZO.[38] Empirical absorption corrections were applied to all data using SORTAV[39] within WINGX.[40] Data collection with the *Australian Synchrotron* was carried out using Blue Ice[41] and initial data processing was carried out using the XDS[42] package. The structures were solved using SHELXS[43] and refined using SHELXL-97[43] within the graphical interface X-SEED.[44]

Acknowledgments

We are grateful to the Australian Research Council (grant DP0984775) and to the Faculty of Science for support and to Monash University for a Postgraduate Publications Award to A. U. Part of this research was undertaken on the MX1 beamline at the Australian Synchrotron, Victoria, Australia.

[1] R. G. W. Hollingshead, *Oxine and its Derivatives, Vol. I*, Butterworths, London, **1954**.
[2] J. P. Phillips, *Chem. Rev.* **1956**, *56*, 271–297.
[3] R. J. Curry, W. P. Gillin, *Appl. Phys. Lett.* **1999**, *75*, 1380–1382.
[4] W. P. Gillin, R. J. Curry, *Appl. Phys. Lett.* **1999**, *74*, 798–799.
[5] a) F. Artizzu, P. Deplano, L. Marchio, M. L. Mercuri, L. Pilia, A. Serpe, F. Quochi, R. Orru, F. Cordella, F. Meinardi, R. Tubino, A. Mura, G. Bongiovanni, *Inorg. Chem.* **2005**, *44*, 840–842; b) F. Artizzu, L. Marchio, M. L. Mercuri, L. Pilia, A. Serpe, F. Quochi, R. Orru, F. Cordella, M. Saba, A. Mura, G. Bongiovanni, P. Deplano, *Adv. Funct. Mater.* **2007**, *17*, 2365–2376.
[6] C. W. Tang, S. A. Vanslyke, *Appl. Phys. Lett.* **1987**, *51*, 913–915.
[7] S. G. Leary, G. B. Deacon, P. C. Junk, *Z. Anorg. Allg. Chem.* **2005**, *631*, 2647–2650.
[8] a) R. Van Deun, P. Fias, P. Nockemann, A. Schepers, T. N. Parac-Vogt, K. Van Hecke, L. Van Meervelt, K. Binnemans, *Inorg. Chem.* **2004**, *43*, 8461–8469; b) R. Van Deun, P. Fias, P. Nockemann, K. Van Hecke, L. Van Meervelt, K. Binnemans, *Eur. J. Inorg. Chem.* **2007**, 302–305.
[9] E. Silina, Y. Bankovsky, V. Belsky, J. Lejejs, L. Peck, *Latv. Kim. Z.* **1997**, 89–92.
[10] M. A. Katkova, Y. A. Kurskii, G. K. Fukin, A. S. Averyushkin, A. N. Artamonov, A. G. Vitukhnovsky, M. N. Bochkarev, *Inorg. Chim. Acta* **2005**, *358*, 3625–3632.
[11] M. A. Katkova, V. A. Ilichev, G. K. Fukin, M. N. Bochkarev, *Inorg. Chim. Acta* **2009**, *362*, 1393–1395.
[12] a) M. Albrecht, O. Osetska, R. Fröhlich, J. C. G. Bünzli, A. Aebischer, F. Gumy, J. Hamacek, *J. Am. Chem. Soc.* **2007**, *129*, 14178–14179; b) M. Albrecht, M. Fiege, O. Osetska, *Coord. Chem. Rev.* **2008**, *252*, 812–824; c) M. Albrecht, M. Fiege, P. Kögerler, M. Speldrich, R. Fröhlich, M. Engeser, *Chem. Eur. J.* **2010**, *16*, 8797–8804; d) M. Albrecht, *Z. Anorg. Allg. Chem.* **2010**, *636*, 2198–2204; e) M. Albrecht, O. Osetska, *Eur. J. Inorg. Chem.* **2010**, 4678–4682; f) J.-C. G. Bünzli, C. Piguet, *Chem. Soc. Rev.* **2005**, *34*, 1048–1077; N. M. Shavaleev, R. Scopelliti, F. Gumy, J.-C. G. Bünzli, *Inorg. Chem.* **2009**, *48*, 2908–2918.
[13] N. M. Shavaleev, R. Scopelliti, F. Gumy, J.-C. G. Bünzli, *Inorg. Chem.* **2009**, *48*, 7937–7946.
[14] G. B. Deacon, P. C. Junk, S. G. Leary, *Z. Anorg. Allg. Chem.* **2004**, *630*, 1541–1543.
[15] G. B. Deacon, C. M. Forsyth, P. C. Junk, U. Kynast, G. Meyer, J. Moore, J. Sierau, A. Urbatsch, *J. Alloys Compd.* **2008**, *451*, 436–439.
[16] G. B. Deacon, C. M. Forsyth, P. C. Junk, A. Urbatsch, *Eur. J. Inorg. Chem.* **2010**, 2787–2797.
[17] G. B. Deacon, C. M. Forsyth, P. C. Junk, S. G. Leary, *New J. Chem.* **2006**, *30*, 592–596.
[18] a) W. J. Begley, M. Rajeswaran, *Acta Crystallogr., Sect. E.* **2006**, *62*, M1200–M1202; b) M. Rajeswaran, W. J. Begley, L. P. Olson, S. Huo, *Polyhedron* **2007**, *26*, 3653–3660.
[19] D. L. Hughes, M. R. Truter, *J. Chem. Soc., Dalton Trans.* **1979**, 520–527.
[20] P. T. Muthiah, S. Murugesan, *J. Coord. Chem.* **2006**, *59*, 1167–1172.
[21] A. J. Middleton, W. J. Marshall, N. S. Radu, *J. Am. Chem. Soc.* **2003**, *125*, 880–881.
[22] S. B. Raj, P. T. Muthiah, G. Bocelli, R. Olla, *Acta Crystallogr., Sect. E.* **2002**, *58*, M513–M516.
[23] S. Francis, P. T. Muthiah, G. Bocelli, A. Cantoni, *Acta Crystallogr., Sect. E.* **2003**, *59*, M1154–M1156.
[24] G. B. Deacon, E. E. Delbridge, D. J. Evans, R. Harika, P. C. Junk, B. W. Skelton, A. H. White, *Chem. Eur. J.* **2004**, *10*, 1193–1204, and references therein.
[25] Cambridge Crystallographic Data Centre v5.32 (including the Feb 2011 update). Several relevant references involving Rb···C interactions are: a) C. S. Weinert, P. E. Fanwick, I. P. Rothwell, *Dalton Trans.* **2003**, 1795–1802; b) C. Eaborn, W. Clegg, P. B. Hitchcock, M. Hopman, K. Izod, P. N. O'Shaughnessy, J. D. Smith, *Organometallics* **1997**, *16*, 4728–4736; c) G. C. Forbes, A. R. Kennedy, R. E. Mulvey, B. A. Roberts, R. B. Rowlings, *Organometallics* **2002**, *21*, 5115–5121; d) M. Niemeyer, P. P. Power, *Inorg. Chem.* **1996**, *35*, 7264–7272.
[26] R. D. Shannon, *Acta Crystallogr., Sect. A* **1976**, *32*, 751–767.
[27] J. H. N. Buttery, Effendy, S. Mutrofin, N. C. Plackett, B. W. Skelton, N. Somers, C. R. Whitaker, A. H. White, *Z. Anorg. Allg. Chem.* **2006**, *632*, 1839–1850.
[28] G. W. Rabe, H. Heise, G. P. A. Yap, L. M. Liable-Sands, I. A. Guzei, A. L. Rheingold, *Inorg. Chem.* **1998**, *37*, 4235–4245.
[29] M. Westerhausen, M. W. Ossberger, J. S. Alexander, K. Ruhlandt-Senge, *Z. Anorg. Allg. Chem.* **2005**, *631*, 2836–2841.
[30] K. Izod, C. Wills, W. Clegg, R. W. Harrington, *Organometallics* **2006**, *25*, 5326–5332.

 © 2011 Wiley-VCH Verlag GmbH & Co. KGaA, Weinheim

[31] W. J. Evans, M. A. Ansari, J. W. Ziller, S. I. Khan, *J. Organomet. Chem.* **1998**, *553*, 141–148.
[32] D. L. Clark, J. C. Gordon, J. C. Huffman, R. L. Vincenthollis, J. G. Watkin, B. D. Zwick, *Inorg. Chem.* **1994**, *33*, 5903–5911.
[33] W. J. Evans, R. Anwander, M. A. Ansari, J. W. Ziller, *Inorg. Chem.* **1995**, *34*, 5–6.
[34] J. M. S. Skakle, J. L. Wardell, S. Wardell, *Acta Crystallogr., Sect. C* **2006**, *62*, O312–O314.
[35] W. S. Loh, M. Hemamalini, H. K. Fun, *Acta Crystallogr., Sect. E* **2010**, *66*, O2907–U2981.
[36] Bruker AXS Ltd, Madison, WI, **2005**.
[37] G. M. Sheldrick, University of Goettingen, Germany, **1996**.
[38] W. M. Z. Otwinowski, *Methods Enzymol.* **1997**, *276*, 307–326.
[39] R. H. Blessing, *Acta Crystallogr., Sect. A* **1995**, *51*, 33.
[40] L. J. Farrugia, *J. Appl. Crystallogr.* **1999**, *32*, 837.
[41] T. M. McPhillips, S. E. McPhillips, H. J. Chiu, A. E. Cohen, A. M. Deacon, P. J. Ellis, E. Garman, A. Gonzalez, N. K. Sauter, R. P. Phizackerley, S. M. Soltis, P. Kuhn, *J. Synchrotron Radiat.* **2002**, *9*, 401–406.
[42] W. J. Kabsch, *Appl. Crystallogr.* **1993**, 795.
[43] G. M. Sheldrick, *Acta Crystallogr., Sect. A* **2008**, *64*, 112–122.
[44] L. J. Barbour, *J. Supramol. Chem.* **2001**, *1*, 189–191.

Received: June 15, 2011
Published Online: August 18, 2011

 © 2011 Wiley-VCH Verlag GmbH & Co. KGaA, Weinheim